JACS
JOURNAL OF THE AMERICAN CHEMICAL SOCIETY
Article
pubs.acs.org/JACS

Electric Field Changes on Au Nanoparticles on Semiconductor Supports – The Molecular Voltmeter and Other Methods to Observe Adsorbate-Induced Charge-Transfer Effects in Au/TiO_2 Nanocatalysts

Monica McEntee,*[,†] Ana Stevanovic,[†] Wenjie Tang,[‡] Matthew Neurock,[†,‡] and John T. Yates, Jr.[†,‡]

[†]Department of Chemistry and [‡]Department of Chemical Engineering, University of Virginia, Charlottesville, Virginia 22904, United States

Supporting Information

ABSTRACT: Infrared (IR) studies of Au/TiO_2 catalyst particles indicate that charge transfer from van der Waals-bound donor or acceptor molecules on TiO_2 to or from Au occurs via transport of charge carriers in the semiconductor TiO_2 support. The $\Delta\nu_{CO}$ on Au is shown to be proportional to the polarizability of the TiO_2 support fully covered with donor or acceptor molecules, producing a proportional frequency shift in ν_{CO}. Charge transfer through TiO_2 is associated with the population of electron trap sites in the bandgap of TiO_2 and can be independently followed by changes in photoluminescence intensity and by shifts in the broad IR absorbance region for electron trap sites, which is also proportional to the polarizability of donors by IR excitation. Density functional theory calculations show that electron transfer from the donor molecules to TiO_2 and to supported Au particles produces a negative charge on the Au, whereas the transfer from the Au particles to the TiO_2 support into acceptor molecules results in a positive charge on the Au. These changes along with the magnitudes of the shifts are consistent with the Stark effect. A number of experiments show that the ~3 nm Au particles act as "molecular voltmeters" in influencing $\Delta\nu_{CO}$. Insulator particles, such as SiO_2, do not display electron-transfer effects to Au particles on their surface. These studies are preliminary to doping studies of semiconductor-oxide particles by metal ions which modify Lewis acid/base oxide properties and possibly strongly modify the electron-transfer and catalytic activity of supported metal catalyst particles.

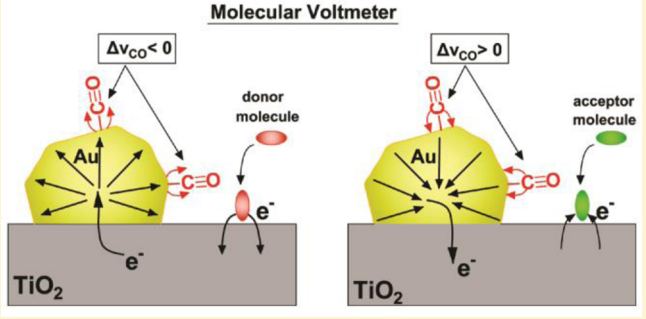

1. INTRODUCTION

The electrical charge that results on supported metal nanoparticle catalysts under reaction conditions is important as it controls electron transfer and catalytic transformations that occur at the active sites on the surface of these particles. Understanding the mechanisms that control charge transfer and the activation of molecules at specific sites can aid in the design of more active and selective catalysts. Charge transfer can occur between adsorbates and different sites on the metal surface as well as between adsorbates and the support. The charge transfer that occurs between atomic sites on the surface with different metal atom coordination numbers provides one of the most prevalent routes whose mechanisms date back to early studies of the work function of atomically smooth metal surfaces compared to atomically rough surfaces as developed by Smoluchowski[1] and Gomer[2] and by Lang and Kohn.[3,4]

In addition to the local charge distribution among metal sites, a metal particle residing on a semiconducting oxide support can also undergo a global charging effect as a result of its electronic interaction with the semiconductor support.[5] As shown in Figure 1, TiO_2 is a semiconductor with a bandgap on the order of 3.1 eV. TiO_2 is typically a nonstoichiometric oxide with a slight deficiency of O^{2-} ions. This leads to upward band bending at the TiO_2 surface, and the TiO_2 is designated as n-type TiO_2 as a result of the extra negative charge that resides at surface oxygen vacancy defects.[5] These vacancy defects and the excess electron charge at the surface are easily observed in STM studies.[6] However, there are also oxygen vacancy-defect electron trap states in the TiO_2 bulk which are located above the Fermi level and slightly below the bottom of the conduction band (CB) which may be partially filled with electrons. These defect sites can participate in accepting or donating electrons to adsorbed donor or acceptor molecules that bind to TiO_2. Adsorbed donor molecules contribute electrons to TiO_2 causing bulk defect sites to become more occupied. In contrast, adsorbed acceptor molecules withdraw electrons from TiO_2 thus resulting in the loss of electrons from these bulk defect sites.[7] The adsorption of donor molecules contributes to a lowering of the extent of upward band bending, while adsorption of an acceptor molecule increases upward band bending.

Au nanoparticles on TiO_2 also respond to charging and discharging of the TiO_2 bandgap defect states by themselves

Received: November 23, 2014
Published: January 22, 2015

DOI: 10.1021/ja511982n
J. Am. Chem. Soc. 2015, 137, 1972–1982

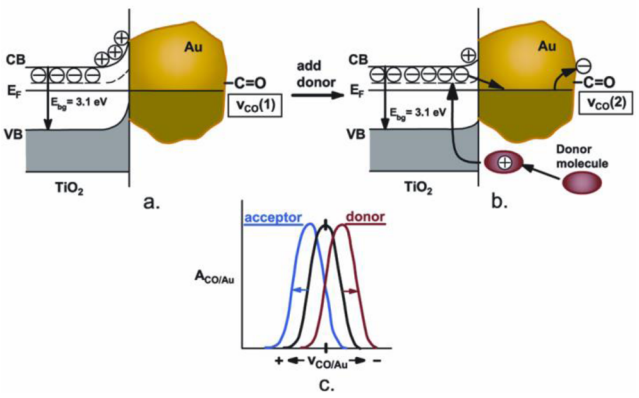

Figure 1. (a and b) Schematic energy levels for TiO_2 and a Au nanoparticle in contact with TiO_2. Electron donation from the donor molecule to a TiO_2 bandgap state is followed by partial electron transfer to the Au particle. Band bending decreases with charge injection from the donor molecule to the support. (c) A chemisorbed CO molecule shifts its ν_{CO} frequency in accordance with the change in electric field caused by changes in the electron surface density at the Au particle. The $\Delta\nu_{CO}$ change is driven in negative and positive directions by donor and acceptor molecules, respectively.

receiving or donating charge to the TiO_2 support depending on the occupancy of these bandgap states. The fractional negative charge on Au nanoparticles will be located at the outer surface of the Au particles as a result of Gauss's law.[8] Changes in the concentration of electron charges on the Au surface will change the electric field at the surface of the Au, and the vibrational spectrum of the chemisorbed CO on Au will therefore shift its ν_{CO} negatively as electron density is added to the Au surface; in contrast, ν_{CO} will shift positively as electron density is removed. These ν_{CO} shifts measure the electric field on metals in accordance with the well-known Stark effect[9] often seen for adsorbates on charged metals.

In Figure 2, electron donation to the bandgap defect states in TiO_2[10] will influence the infrared (IR) broadband absorbance

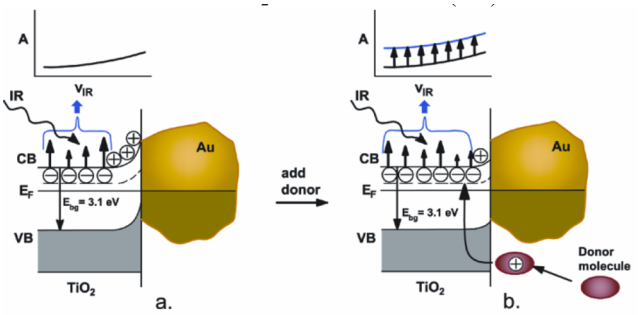

Figure 2. Adsorption of a donor molecule onto n-type TiO_2 results in a reduction in upward band bending and an increase in the population of the gap states near the bottom of the CB. This is detected by an enhancement of background absorbance of TiO_2 in the IR region as a result of IR excitation from the gap states into continuum CB states.

of the background of the TiO_2 IR spectrum, and this may be sensitively observed by transmission IR. An increase (or decrease) in electron occupancy in the bandgap states causes an increase (or decrease) in the background absorbance in the IR spectrum of the catalyst support. Figure 2 shows a schematic in which electrons are excited by IR photons from the TiO_2 bandgap states over a wide frequency range leading to excitation into the continuum of the TiO_2 CB states.

The role of the adsorption of donor and acceptor molecules on TiO_2 is schematically shown in Figure 3, where the extent of

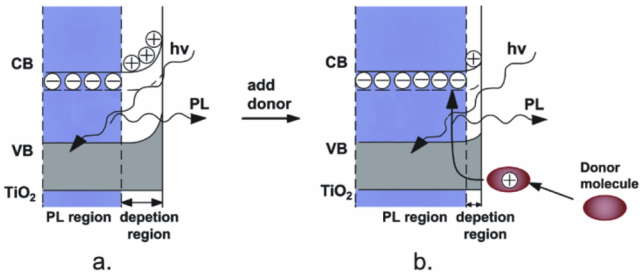

Figure 3. Schematic diagram showing the band bending influence of the adsorption of donor molecules on an n-type TiO_2 substrate. An increase in thickness of the PL source region by donor molecule adsorption causes the PL intensity to increase.

the TiO_2 bend banding that results from molecule adsorption is correlated with the intensity of emission of photoluminescence (PL) from the semiconductor TiO_2. The depth region which contains curved upward band bending leads to a rapid separation of photoexcited and oppositely moving electrons and holes, and therefore, prevents PL by electron−hole recombination. This depth region of band bending is called the depletion region where activated negative and positive charge carriers rapidly move away from each other preventing recombination and PL emission. Photons incident on the TiO_2 surface can only produce PL from depths further beneath the depletion region as shown in the blue area in Figure 3. Hence, the reduction of both the degree of band bending and the width of the depletion region by adsorption of a donor molecule will be accompanied by an enhancement of the PL intensity.[11,12] The separate PL measurement of the opposite influence of electron-donor and electron-acceptor molecules on charge distribution in TiO_2 correlates well with the TiO_2 charging effects and subsequent electron transfer to Au nanoparticles as observed by the other spectroscopic methods in Figures 1 and 2. It has been observed that small Au particles readily retard PL for Au/TiO_2 catalysts due to metal supported carrier particles being recombined in Au without photon emission.[13]

This paper examines the small charging effects induced by physically adsorbed molecules on a semiconducting TiO_2 support containing Au nanoparticles. Physically adsorbed donor or acceptor molecules influence the electronic properties of the TiO_2 support, and this influence is rapidly passed to Au metal nanoparticles by charge-transfer effects. The modified Stark effect has been measured previously for diatomic molecules such as chemisorbed CN on Ag electrodes and for CO on Pt, Au and other transition metal electrodes in electrolytes.[14−16] The large fields that exist in the electrical double layer of a few Å depth above the metal surface,[16] as well as for chemisorbed CO in vacuum,[14,17] and the sign and magnitude of the Stark shift that appear in these systems have been correlated to both the sign as well as the magnitude of the applied electrical field.[15,18] The Stark effect has been used recently, in addition to the field of electrochemistry, in the areas of nanomaterial antennas, sensors, and plasmonic resonance studies.[19,20] In these studies, linear Stark shifts of CO are used to gauge the large local electric fields. The experiments reported here are carried out at temperatures where physical adsorption

DOI: 10.1021/ja511982n
J. Am. Chem. Soc. 2015, 137, 1972−1982

of the adsorbed donor or acceptor molecules occurs only on the oxide support. Relatively small charge effects on the support are observed with several independent spectroscopic methods, along with the associated Stark effect for adsorbed CO on Au.

The sign of the donor or acceptor charging effect measured on TiO_2 for the PL and IR behavior agrees in all three measurements. The agreement between three measurement methods for measuring the sign and magnitude of charge transfer from a physisorbed donor or acceptor molecule to the TiO_2 support and then to supported Au nanoparticles on TiO_2 leaves little doubt that small electron-transfer effects are spectroscopically measurable on metal/semiconductor catalysts by multiple spectroscopies.

Other methods, such as surface-enhanced Raman spectroscopy (SERS) and picosecond laser flash photolysis experiments,[21−23] have also been used to measure electron transfer in nanomaterials, where the techniques themselves induce electron mobility. However, this article describes three unique methods that measure the electron transfer induced not by the light source, but by the adsorbed molecules on the surface. This effect may have a great importance on a catalyst which is not being exposed to light; a catalyst being exposed to a metal oxide support which has been chemically modified for enhancement of catalytic activity.

The studies reported here provide insights as to how changes in oxide properties that result from changes in its chemical composition and its Lewis acidity or via adopting mixed (or doped) semiconducting oxides[24,25] influence the charge transfer into and out of the catalyst.

2. EXPERIMENTAL AND THEORETICAL METHODS

2.1. Catalysts and Gases. The Au/TiO_2 catalyst was synthesized using the precipitation−deposition method provided by Zanella et al.[26] in order to obtain ∼3 nm diameter Au particles of approximately 8 wt %.[27,28] The powdered TiO_2 is Degussa P25 containing a mixture of ∼70% anatase and 30% rutile phases acquired from Evonic Industries. The TiO_2 average particle size is ∼50 nm, and the surface area of the TiO_2 is 60 $m^2\ g^{-1}$.[29,30] A high-resolution TEM image of the ∼3 nm Au/TiO_2 catalyst is shown in Figure S1 showing that crystalline Au particles are present on TiO_2 surfaces, which also display TiO_2 characteristic crystal structure seen by TEM. Au/SiO_2 catalyst samples already synthesized using the same method and characterized as having the same size ∼3 nm diameter Au particles were also provided by Zanella.[31] CO (99.9% purity, Matheson Tri-Gas), CH_4 (>99% purity), C_2H_6 (99.999% purity, Matheson Tri-Gas), C_3H_8 (99.999% purity, Matheson Tri-Gas), and SF_6 (99.8% purity) were all further purified using a N_2(lq) trap attached to a stainless steel high-vacuum storage and transfer line before introducing each gas into the reaction cell.

2.2. IR Measurements. The vacuum IR cell employed for these experiments has a base pressure of 1.0×10^{-8} Torr and is described in detail elsewhere.[28,32] Before every experiment, the Au/TiO_2 catalyst was heated to 680 K in O_2(g) for 30 min in order to remove any accumulated hydrocarbon impurities and then cooled down to 105 K. Approximately 60 mTorr of CO was introduced into the cell to achieve CO saturation adsorption, and then 5 min later the CO(g) was evacuated for 10 min. The catalyst was then systematically heated up to 200 K in order to desorb CO only from the TiO_2 support leaving CO chemisorbed on the Au nanoparticles. After 3 min at 200 K, the catalyst was cooled down to the desired adsorption temperature used for the addition of modifier molecules. After 15 min at constant temperature, the desired donor or acceptor gas was added to the cell in increments until saturation coverage was observed by FTIR of the donor or acceptor molecules on the TiO_2 or SiO_2 support. The FTIR spectrum was taken for each increment of gas added with an average of 128 scans at 2 cm^{-1} resolution. Once the catalyst was saturated with either the donor or acceptor molecule, an additional spectrum was obtained every minute for 10 min. Then, the catalyst was heated up in vacuum (or in partial pressure for CH_4) in 5 K increments starting from the adsorption temperature in order to remove the adsorbates in small increments from the support. An IR spectrum was taken for each of these treatment temperatures as well, showing that CO IR line shifts and donor/acceptor absorption spectra exhibit reversible behavior in each case as donor or acceptor molecules are added or removed.

In addition to measuring the vibrational behavior of CO when influenced by the physisorbed donor or acceptor molecules used to modify the Au/TiO_2 catalysts, we employed the IR background shift (see Figure 2) which extends from about 4000 to ∼1000 cm^{-1} when varied electron transfer to or from the TiO_2 is caused by addition or removal of donor or acceptor molecules. It was found that this shift could be measured most easily by observations of the TiO_2 background intensity at 1900 cm^{-1} or over the 1800−2000 cm^{-1} region, where all vibrations of adsorbed species are missing.

2.3. PL Measurements. Photoluminescence measurements were performed in an IR/PL stainless steel cell under high-vacuum conditions. The base pressure of the cell was 2.0×10^{-9} Torr after bakeout. More detailed information about the IR/PL set up can be found elsewhere.[11] For the PL measurements, the 320 ± 10 nm (3.88 eV) excitation light was selected from a pulsed Xe source which focused power measured over time at the sample position of 9.1×10^{-5} J s^{-1} cm^{-2} (1.5×10^{14} photons cm^{-2} s^{-1}). The emitted PL light was collected by an R928 photomultiplier tube covering the range of 200−900 nm. The PL spectra were plotted employing a scan speed rate of 500 nm·min^{-1}. To minimize the specular reflection of the incident light from a CaF_2 window, all the spectra were collected 15° off a specular direction of the source light, and a 390 nm cut off filter was employed.

Before each PL experiment, the TiO_2 sample was cleaned by heating in vacuum to 680 K and then introducing 0.8 Torr of O_2 for 25 min at 680 K to remove all hydrocarbon impurities. After evacuation of O_2 at 680 K, the sample was cooled down to l−N_2 temperatures for PL measurements. During gas adsorption experiments, the excitation light was blocked by a shutter to avoid any influence of UV light. The surface was modified by sequential addition of known amounts of gas into the system. Following surface modification by electron-donor or electron-acceptor adsorbate molecules the surface was exposed to UV light for only 67 s to collect the PL spectra, and separate experiments show that this small UV exposure did not appreciably change the PL intensity.

2.4. DFT Model and Parameters. First principle density functional theory (DFT) calculations were carried out to gain insights into charge transfer between Au nanoparticles and the TiO_2 support and the changes in the CO frequency shifts for CO bound to Au/TiO_2 that occur upon the adsorption of donor and acceptor molecules on the TiO_2 support. A model Au/TiO_2 catalyst was constructed by bonding a gold nanorod 3 atomic layers high and 3 atomic layers wide to the most stable rutile TiO_2(110) surface. This supported gold nanorod model has been used successfully in a number of previous theoretical studies to mimic the properties and reactivity of Au on different supports.[27,28,33−35] The TiO_2 support was modeled using a (2 × 3) and (4 × 3) surface unit cell comprised of three O−Ti−O trilayers. A (4 × 3) Au/TiO_2 structure was used to calculate the effect of adsorbates on TiO_2 remote from the Au perimeter, while (2 × 3) Au/TiO_2 was used for the rest of calculations. The top half of the TiO_2 was fully relaxed whereas the bottom half was held fixed to the bulk TiO_2 lattice.

All of the DFT calculations reported herein were carried out using the Vienna Ab Initio Software Package (VASP)[36] program with a plane-wave basis set with cutoff energies of 400 eV and pseudopotentials constructed in projector augmented-wave (PAW) framework.[37,38] The PW91 gradient approximation (GGA) functional was used to model the exchange−correlation effects.[39] The DFT+U method was implemented to better describe the on-site Coulomb interactions in TiO_2.[40] The value of U was chosen to be 4.0 eV as it produced an optimal match of band features observed experimentally.[41] Spin polarization was included for all calculations. A 10 Å

DOI: 10.1021/ja511982n
J. Am. Chem. Soc. 2015, 137, 1972−1982

vacuum gap was used in the z-direction for the Au/TiO_2 model to prevent any image−image interactions caused by the periodic boundary condition. The (2 × 3) and (4 × 3) Au/TiO_2 surfaces were sampled with a (2 × 2 × 1) and (1 × 2 × 1) k-point mesh, respectively.[42] Dispersion was included in the calculations to consider the weak interactions between adsorbates and the Au/TiO_2 surface.[43] Geometries were considered optimized when the forces on each atom were <0.03 eV/Å. The charge associated with each atom was subsequently calculated using the Bader analysis.[44,45]

3. RESULTS

3.1. IR CO Frequency Shifts using Donor and Acceptor Adsorbate Molecules on Au/TiO_2. The first experiment is shown in Figure 4a displaying CO adsorbed on Au at 140 K on a Au/TiO_2 catalyst before the addition of C_3H_8 donor molecules to TiO_2 (black curve). The absence of an absorbance band at 2179 cm^{-1} assigned to CO adsorbed on TiO_2 shows that CO is not adsorbed on the support following CO desorption at 200 K.[27,46] The main absorbance band at ~2123 cm^{-1} is assigned to CO on metallic Au^0 sites and the shoulder at 2141 cm^{-1} is assigned to CO on $Au^{\delta+}$ sites.[27,46−48] From the width of the ν_{CO} band, it is likely that a superposition of CO frequencies exists characteristic of several different types of Au adsorption sites present on the Au nanoparticles. Incremental amounts of C_3H_8 were then added to the Au/TiO_2 catalyst at 140 K. Based on C_3H_8 and other light alkane temperature-programmed desorption experiments along with thermodynamic studies on Au (and Pt) single crystals and TiO_2 (and V_2O_3) oxides separately, C_3H_8 desorbs from Au below 140 K and remains adsorbed on TiO_2 at the same temperature.[49−52] After each addition of C_3H_8 on TiO_2, an IR spectrum was taken as shown in Figure 4a (gray curves). The major C−H stretch absorbance bands of propane on TiO_2 are 2964 cm^{-1} ($\nu_{as}(CH_3)$), 2944 cm^{-1} ($\nu_{as}(CH_2)$), and 2876 cm^{-1} ($\nu_s(CH_2)$) as shown in the insets of Figure 4.[53] Control experiments involving only C_3H_8 were performed on the pure TiO_2 catalyst as well, and the same C−H absorbance bands were observed indicating that the C_3H_8 molecules were adsorbed only on the TiO_2 support. The red curves in both the CO/Au and C_3H_8/TiO_2 IR regions represent the TiO_2 catalyst support saturated with C_3H_8 in Figure 4a. Saturation of the catalyst by C_3H_8 is determined by measuring the integrated absorbance of the C−H band intensity. Once the C−H bands stop growing even though more molecules are being added to the cell, the TiO_2 support is deemed to be saturated with C_3H_8 at 140 K and ν_{CO} shifts are sensitive only to adsorbed C_3H_8. As seen from the CO/Au IR bands, the frequencies for CO on both Au^0 and $Au^{\delta+}$ sites redshift toward lower frequencies as C_3H_8 is added to the TiO_2 support indicating partial electron transfer from the C_3H_8 to the support and then to the Au.

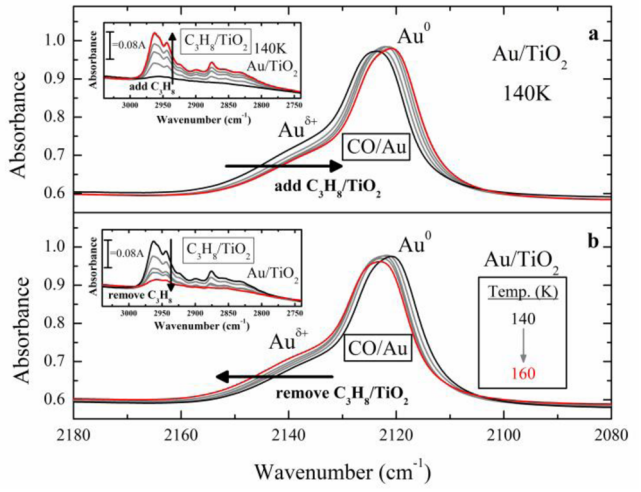

Figure 4. IR spectra of CO on Au as C_3H_8 (a) increases in coverage on TiO_2 to saturation (red curve) at 140 K and (b) decreases in coverage on TiO_2 starting at saturation (black curve) and nearing complete desorption (red curve) after heating in small temperature intervals up to 160 K. A reversible shift in the broad ν_{CO} feature is observed as caused by adsorption and desorption of C_3H_8 donor molecules on the TiO_2 support. The corresponding insets are the IR C−H stretching spectral region of physisorbed C_3H_8 on TiO_2 during (a) addition at 140 K and (b) removal in the range of 140−160 K. C_3H_8 exhibits reversible adsorption/desorption behavior.

After C_3H_8 saturation (black curves in Figure 4b), the catalyst was heated in vacuum in 5 K steps (gray curves) until the majority of the C_3H_8/TiO_2 was removed (red curves). As shown in Figure 4b, as C_3H_8 was removed from the TiO_2 surface, the CO/Au absorbance band blueshifts back to the original frequency, ~2123 cm^{-1}, observed before C_3H_8 adsorption. The reversibility of the CO frequency shifts suggests no chemical decomposition of the adsorbates and indicates that a reversible electron transfer occurs to and from the Au particles, induced by the physisorbed C_3H_8 donor molecules on the TiO_2 support.

Similar experiments were performed using an acceptor molecule, SF_6, in order to produce an opposite electron transfer between Au and the TiO_2 support. Figure 5a shows the CO/Au absorbance bands before SF_6 adsorption (black curves) and after incremental additions of SF_6 (gray curves) until SF_6 saturation (red curves) occurs at 140 K. The inset in Figure 5a displays an absorbance band of physisorbed SF_6 at 946 cm^{-1}. Gas phase SF_6 has a similar absorbance band at 948 cm^{-1} indicating only weak SF_6 van der Waals interactions and

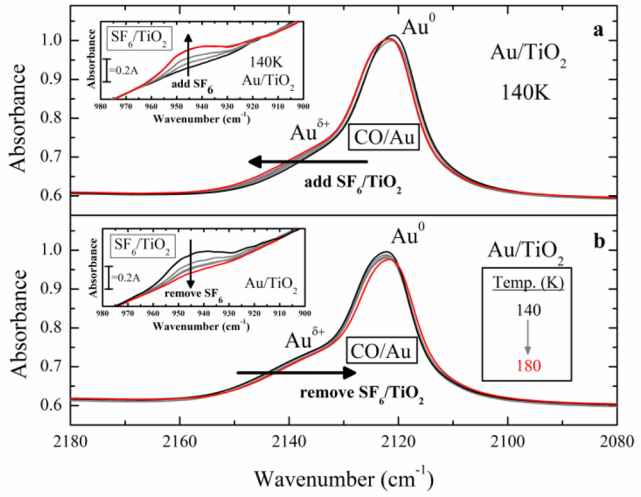

Figure 5. IR spectra of CO on Au as SF_6 (a) increases in coverage on TiO_2 to saturation (red curve) at 140 K and (b) decreases in coverage on TiO_2 starting at saturation (black curve) and nearing complete desorption (red curve) after heating up to 180 K. A reversible shift in the broad ν_{CO} feature is observed as caused by adsorption and desorption of SF_6 acceptor molecules on the TiO_2 support. The corresponding insets are the IR spectral region of SF_6 on TiO_2 during (a) addition at 140 K and (b) removal in the range of 140−180 K. SF_6 exhibits reversible adsorption/desorption behavior.

DOI: 10.1021/ja511982n
J. Am. Chem. Soc. 2015, 137, 1972−1982

binding to the Au/TiO_2 catalyst.[54] As with C_3H_8, SF_6-TPD experiments on Au single crystals and separately on metal oxides verify that SF_6 adsorbs only on TiO_2 under the experimental conditions employed here.[55,56] As shown in Figure 5a, when SF_6 is adsorbed on TiO_2, the CO/Au IR frequency shifts upward toward higher frequencies opposite to the effect observed when C_3H_8 adsorbs on TiO_2. Furthermore, when the catalyst is subsequently heated in 5 K increments up to 180 K starting from SF_6 saturation (Figure 5b, black curve) and ending with a clean TiO_2 surface (Figure 5b, red curve), the CO/Au IR frequency exhibits reversed redshifts toward lower frequencies opposite to the blueshift observed for C_3H_8 desorption.

In order to prove this IR shift phenomenon is not just specific to C_3H_8 and SF_6 molecules, similar experiments were performed using methane, CH_4, and ethane, C_2H_6, donor molecules. The experimental CO/Au IR frequency differences before and after molecular adsorption were plotted versus adsorbate coverage on Au/TiO_2 as shown in Figure 6a. Each

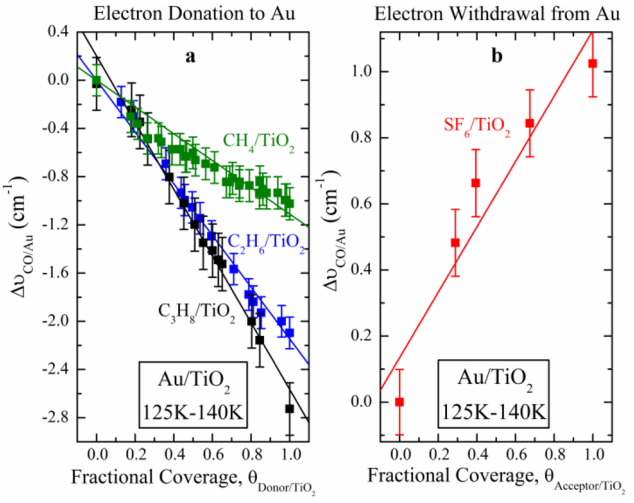

Figure 6. IR CO/Au frequency shifts vs adsorbate coverage on TiO_2 support for (a) donor molecules CH_4 (green squares), C_2H_6 (blue squares), and C_3H_8 (black squares) and (b) acceptor molecule SF_6 (red squares). The analytically determined errors in the measurements of $\Delta\nu_{CO/Au}$ are discussed in Section 3.1.

centered maximum frequency of the CO on Au was subtracted from the frequency of the CO spectrum without donor or acceptor molecule adsorption to obtain the vibrational shifts. The CO spectral bands were fit to Lorentzian distribution functions to obtain the shift error bars shown in Figure 6a,b. Then, the integrated C−H or S−F absorbance band area for each spectrum was normalized to full-coverage spectra to yield the fractional coverage of the donor or acceptor adsorbate on the support. For CH_4, C_2H_6, and C_3H_8 adsorbed on Au/TiO_2, the maximum CO/Au IR shifts per monolayer of donor molecule are negative by ~1.0 cm^{-1} (Figure 6a, green squares), ~2.0 cm^{-1} (Figure 6a, blue squares), and ~2.8 cm^{-1} (Figure 6a, black squares), respectively. For SF_6 adsorbed on Au/TiO_2, the maximum CO/Au IR shift is positive by ~1.0 cm^{-1} (Figure 6b, red squares).

The overall absolute frequency shifts for SF_6 adsorption and desorption are smaller than for C_3H_8-induced frequency shifts. The small shifts for SF_6 compared to C_3H_8 are most likely due to the fact that Au/TiO_2 is an n-type semiconductor with an overall negative charge present on the surface before SF_6 adsorption. Thus, the negative charge character of the TiO_2 surface repels the electronegative SF_6 molecules and lowers the efficiency of electron transfer upon adsorption on TiO_2.

In order to further eliminate the possibility of CO IR shifts being caused by nearby CO interactions with C_3H_8 or SF_6 on Au sites, identical experiments were done on a Au/SiO_2 catalyst (Figure 7). Both the donor molecule, C_3H_8 (Figure 7a), and the acceptor molecule, SF_6 (Figure 7b), adsorb on SiO_2.

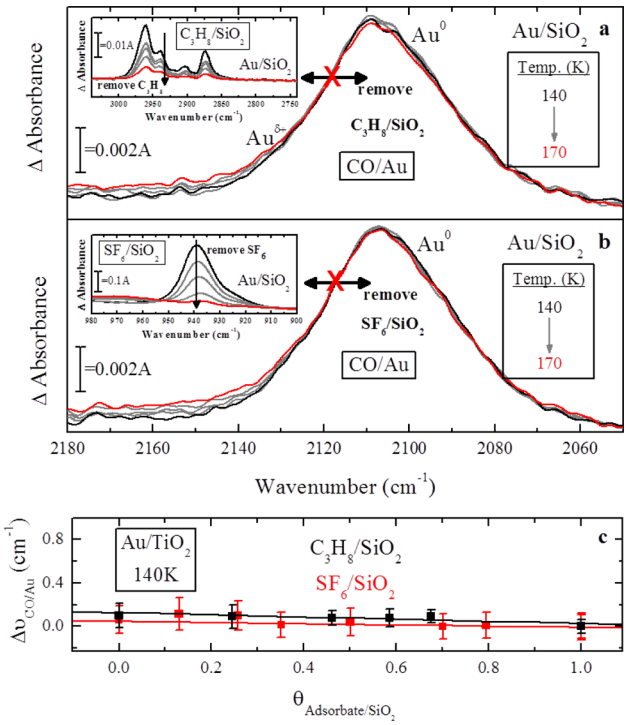

Figure 7. IR spectra of CO on Au/SiO_2 as (a) C_3H_8 and (b) SF_6 decrease in coverage on SiO_2 starting at saturation (black curve) and nearing complete removal (red curve) after heating up to 170 K. The corresponding insets are the IR spectral region of (a) C_3H_8 and (b) SF_6 on SiO_2 during removal in the range of 140−170 K. (c) The absence of IR CO/Au frequency shifts vs donor or acceptor molecule adsorption on SiO_2.

However, neither molecule induced a significant frequency shift in the CO/Au IR frequencies. For C_3H_8 and SF_6 adsorbed on Au/SiO_2, Figure 7c shows that the total $CO/Au/SiO_2$ IR shifts are very small or zero compared to measuring the CO frequency shifts on Au/TiO_2 (Figure 6). The absence of detectable CO/Au IR shifting on Au/SiO_2 compared to similar measurements on Au/TiO_2 shows that the electron-transfer interaction between Au and the support oxide requires that the oxide be a semiconductor with an appreciable level of charge carriers. Insulator covalent oxides, such as SiO_2, do not possess appreciable charge carriers to influence supported Au particles. Furthermore, the comparison of the results for Au/SiO_2 with those on Au/TiO_2 helps to eliminate the possibility that $\Delta\nu_{CO}$ depends on donor/acceptor molecules on Au.

3.2. Electron Transfer to and from Au/TiO_2 as Observed from Defect Site Electron Population in the Energy Gap of TiO_2. It is well-known that defect sites in the bulk, or on the surface of TiO_2, will interact with electron-donor/acceptor molecules. The charge received or donated from adsorbed molecules causes a variation in the population of charge in these defect sites. The defect sites are close to the

DOI: 10.1021/ja511982n
J. Am. Chem. Soc. 2015, 137, 1972−1982

bottom of the CB in TiO_2. Therefore, when the sites are filled with electrons, they participate in the absorption of IR radiation causing higher levels of electron excitation to occur from the defect into the TiO_2 CB. This absorption occurs over a broadband due to the energy continuum of CB states which may be occupied by IR excitation of defect-bound electrons, and a broad background IR absorption from near 1000 to 4000 cm^{-1} is observed. Similar effects have been seen by others on TiO_2.[57−60] This process has been observed also for ZnO[61] and is termed "metallization" as a result of the IR-induced electronic excitation into the continuum in the CB. Atomic H adsorbed on TiO_2 behaves as an electron donor resulting in additional electron occupancy of the defect states and a growth in the broad IR absorbance.[59,60] The IR absorbance due to electronic population of defect sites in single crystal rutile-TiO_2(110) has recently been attributed, in part, to the excitation of hydrogenic polaronic states which are associated with a series of sharp superimposed absorbance bands observed on top of the broad-band absorbance caused by defect bound electron excitation into the CB continuum.[62] This phenomenon is also observed for Au/TiO_2 catalysts during the adsorption of physically absorbed donor or acceptor molecules on the TiO_2 support and is therefore coupled to Stark shifting of CO/Au species.

Figure 8 shows the shift of the background IR spectrum for Au/TiO_2 catalysts due to donor molecules as a function of the

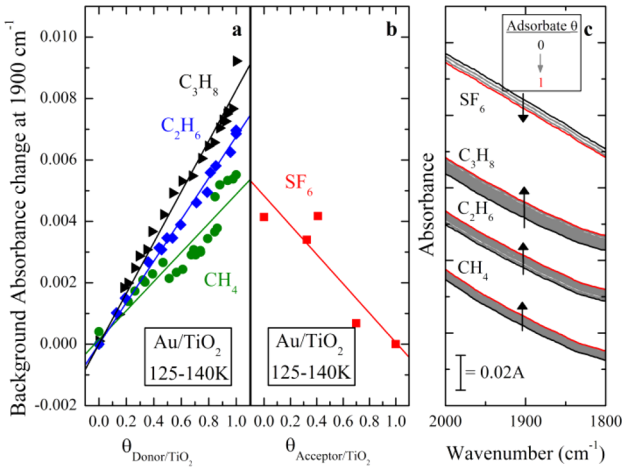

Figure 8. (a) The background IR absorbance changes measured at 1900 cm^{-1} for C_3H_8, C_2H_6, and CH_4 donor molecules. (b) The opposite shift occurs for the SF_6 acceptor molecule. (c) Partial spectra of the background absorbance over 1800−2000 cm^{-1} for adsorption of both donor and acceptor molecules.

adsorption coverage of the donor molecules on TiO_2. The broad band responds by moving upward upon electron donation from the physically adsorbed molecules employed. This broad shift can be monitored by the motion of the background absorption as monitored by the changes in the band at 1900 cm^{-1}. Figure 8a shows the increase in the background absorbance at 1900 cm^{-1}, when three different donor molecules (CH_4; C_2H_6; C_3H_8) are systematically and separately adsorbed. Figure 8b shows the decrease in the background absorbance when an acceptor molecule (SF_6) is adsorbed on TiO_2. Figure 8c shows the observed spectral background over a broader region (1800−2000 cm^{-1}) as it shifts up or down when either donor or acceptor molecules are adsorbed on the Au/TiO_2 catalyst.

3.3. Redistribution of Electronic Charge in TiO_2 causing Band Bending by Donor or Acceptor Adsorbate Molecules − PL Effects. The adsorption of donor or acceptor molecules on a semiconducting-TiO_2 surface produces a dramatic change in the intensity of PL from the surface as a result of band bending in the surface region.[11,12,63] TiO_2 is an n-type semiconductor where oxygen-vacancy surface defects result in the buildup of negative charge on the clean surface. This extra surface negative charge causes the conduction and valence band edges to bend upward as shown in Figure 3.[5] Upward band bending increases the thickness of the depletion region associated with the curved upward bent bands. In the depletion region, PL is eliminated since the large motion in opposite directions of photogenerated electrons and holes sweeps the surface depletion region free of recombining charges before charge recombination (and associated PL) can occur. Hence, enhanced band bending may be detected from the change in PL intensity when donor or acceptor molecules are adsorbed.[11] When n-type TiO_2, with initially upward bent bands, adsorbs donor molecules, the bands bend downward resulting in an increase in PL intensity; the opposite band bending occurs for the adsorption of acceptor molecules on n-type TiO_2.

Figures 9 and 10 show the behavior of the PL spectra and PL intensity, respectively, from clean powdered TiO_2 which has

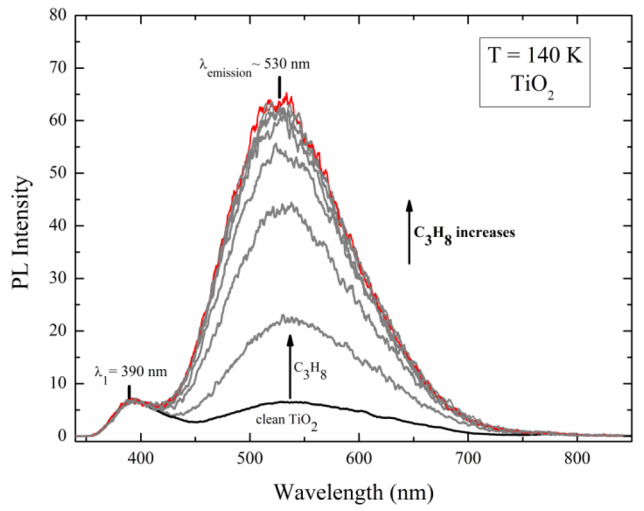

Figure 9. PL intensity of a clean TiO_2 surface upon adsorption of C_3H_8 at 140 K. The main peak at ~530 nm of a clean TiO_2 (black spectrum) increases upon addition of adsorbed C_3H_8 (gray spectra) reaching a saturation point (red spectra). The small light peak at λ_1 = 390 nm is due to a constant light reflection effect which is always present at a constant level and is disregarded.

then been treated with physically adsorbed C_3H_8 donor molecules or with physically adsorbed SF_6 acceptor molecules. Figure 9 shows the change in the PL spectra of a clean TiO_2 surface upon adsorption of C_3H_8 at 140 K. The peak at ~530 nm corresponds to PL emission as a result of electron−hole recombination in TiO_2. The feature at 390 nm originates from a small portion of the reflected source light from a CaF_2 window and is invariant during the experiments. The resulting increase in PL intensity at ~530 nm for the donor-C_3H_8 molecule is consistent with reduction of the surface depletion region thickness. For acceptor SF_6 molecules, the surface

DOI: 10.1021/ja511982n
J. Am. Chem. Soc. 2015, 137, 1972−1982

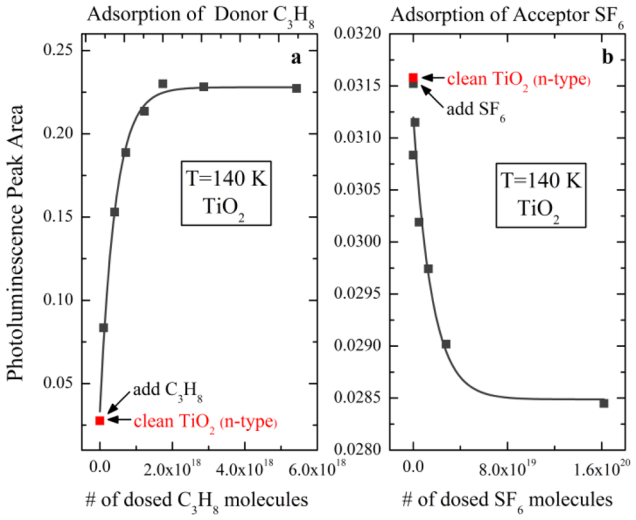

Figure 10. Opposite effects of van der Waals bound donor-C_3H_8 (a) and acceptor-SF_6 (b) molecules on the magnitude of PL intensity. (a) The results indicate that donor-C_3H_8 molecules reduce upward band bending in n-type TiO_2, causing an increase in PL intensity. (b) Conversely, acceptor-SF_6 molecules enhance upward band bending in n-type TiO_2, causing a decrease in PL intensity.

depletion region grows thicker, causing diminished PL intensity.

3.4. DFT Calculations of IR CO/Au Frequency Shifts by Donor and Acceptor Molecules Adsorbed on the TiO_2 Support. The adsorption of the CH_4, C_2H_6 and C_3H_8 donor molecules onto Ti sites on TiO_2 at the Au/TiO_2 perimeter result in theoretically calculated CO/Au frequency shifts that are negative by 2, 3, and 5 cm^{-1}, respectively (Figure 11b–d). A detailed analysis of charge density differences before and after the adsorption of the donor molecules on TiO_2 shows that the donor molecules induce an increase of electron density on the Au particle, resulting in negative charge on Au surface sites. The charge on the Au site to which CO is adsorbed is −0.02, −0.03, and −0.04 e for CH_4, C_2H_6, and C_3H_8 adsorption on the TiO_2 support, respectively (Figure 11b–d). The CO/Au frequency shift for the SF_6 acceptor molecule adsorbed onto the TiO_2 support at the Au/TiO_2 interface is positive by 2 cm^{-1} (Figure 11e). The adsorption of SF_6 on TiO_2 induces a decrease in electron density on the Au particle, resulting in positive charge on Au sites. The charge on the Au site to which CO is bound increases from −0.02 e (CH_4) to +0.03 e if SF_6 is adsorbed on TiO_2 instead (Figure 11e). The trend of the calculated CO/Au frequency shift is consistent with all of our experimental observations for donor and acceptor molecules on TiO_2. As shown in Figure 12, a CH_4 donor adsorbate located further away from the Au perimeter induces a smaller IR CO/Au frequency shift; however, since shifts still occur, the electron transfer has to occur through the TiO_2 to the Au instead of through space from the donor or acceptor on the TiO_2 directly to the Au and adsorbed CO molecule. CH_4 that adsorbed ~6 Å away from the Au perimeter results in a negative $\Delta\nu_{CO}$ of 1 cm^{-1}, as shown in Figure 12b. The electron density perturbations caused by all of the donor molecules and by the SF_6 acceptor molecule are observed in the TiO_2, and this charge effect is transmitted through the TiO_2 to Au and then to the C–O bond of Au-CO species. The charge on the Au site to which CO is adsorbed on is −0.01 e in the case of CH_4 located ~6 Å away from the Au. CO molecules that are remote from

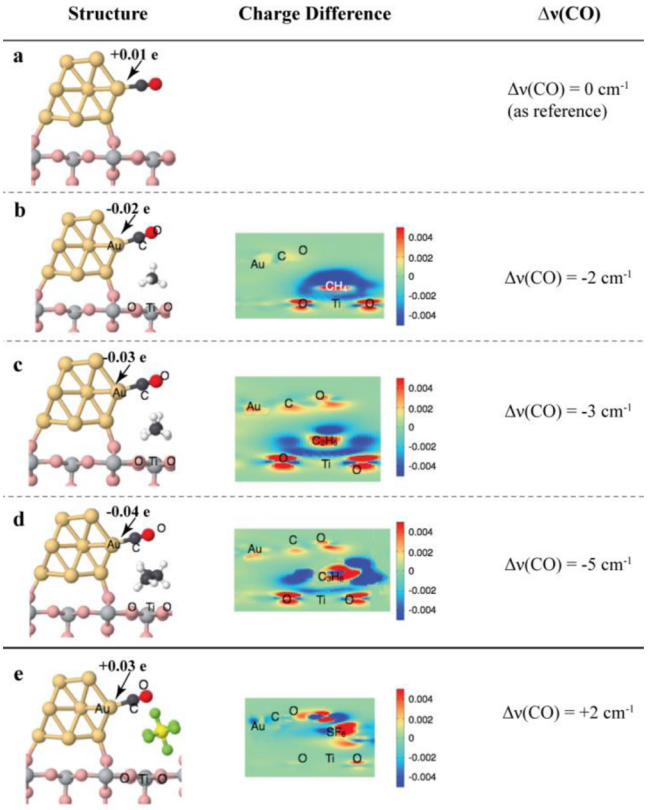

Figure 11. (a) Adsorption of CO on Au supported on TiO_2 and the resulting charge on the Au. CO frequency shift with the adsorption of (b) CH_4, (c) C_2H_6, (d) C_3H_8, and (e) SF_6. The charge on the Au atom is indicated in the figure. The Au atoms, Ti atoms, the O in the TiO_2 lattice, adsorbed O, C atoms, H atoms, F atoms, and S atom are shown in gold, gray, pink, red, black, white, green, and light yellow, respectively. Charge density differences before and after donor and acceptor adsorption are shown in the second column spatial figures. Orange and red indicate increasing of electron density, while green and blue indicate decreasing electron density.

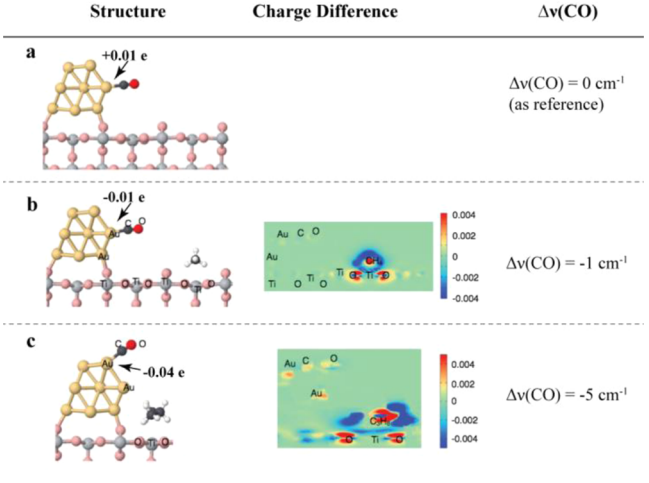

Figure 12. (a) Adsorption of CO on Au supported on TiO_2 and the resulting charge on the Au. CO frequency shift with the adsorption of (b) CH_4 that is remote from the perimeter; and (c) C_3H_8 when CO is remote from the perimeter. The charge on the Au atom is indicated in the figure. Charge differences before and after CH_4 and C_3H_8 adsorption are shown in the second column spatial figure. Orange and red indicate increasing of electron density, while blue indicates decreasing electron density.

DOI: 10.1021/ja511982n
J. Am. Chem. Soc. 2015, 137, 1972–1982

the perimeter exhibit similar frequency shifts as those CO molecules adsorbed near the perimeter. As shown in Figure 12c, a frequency shift of −5 cm^{-1} is found for CO on top sites of the Au/TiO_2 model. This shift is the same as the CO/Au frequency shift in Figure 11d where CO is adsorbed near the perimeter. Thus, electrons transferred to or from Au cause a field effect which is similar over the entire Au outer surface, i.e., a Stark effect.

4. DISCUSSION

4.1. Three Spectroscopic Methods for Observing Charge-Transfer Effects: Au/TiO_2 Catalysts. Three spectroscopic methods have been employed to understand the redistribution of electrons in a Au/TiO_2 catalyst due to the physisorption of donor or acceptor molecules on the TiO_2 support. Each method demonstrates that donor and acceptor molecules differ in the direction of electron transfer which is induced from TiO_2 to Au. While electron transfer into the semiconducting TiO_2 support is effective, similar donor and acceptor experiments with insulator SiO_2 supports are ineffective in producing electron transfer from the donor or acceptor molecules. Measurable $\Delta\nu_{CO}$ effects do not occur on Au/SiO_2.

For ∼3 nm diameter Au particles bound to a TiO_2 support, the redistribution of electrons in the support may be determined by observing small spectroscopic shifts in the C−O stretching motion for chemisorbed CO on the Au surface. The average ∼3 nm Au−Au particle separation is at least ∼40 Å, based on a 0.15 fraction coverage of the TiO_2 particles as measured by TEM.[13] Beyond a Au particle−particle separation of ∼6 Å, the interparticle spectroscopic effect for adsorbed CO involves less than a 1 cm^{-1} shift in the ν_{CO}. Figure 13 shows a schematic diagram of the electron-transfer effect from a donor molecule to the TiO_2 support and then to the contacting Au nanoparticle containing chemisorbed CO molecules. This phenomenon is produced by a composite metal/semiconductor nanomaterial which we term a "molecular voltmeter" as schematically shown in Figure 13. Electrons transferred to or from the metal particle cause the CO frequency to shift to lower frequency (caused by donor molecules) or to higher frequency (caused by acceptor molecules), in accordance to a Stark shift.

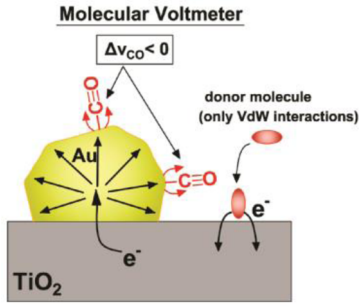

Figure 13. Schematic representation of the molecular voltmeter for the measurement of charge transfer from donor molecule to semiconducting TiO_2 support and then to a supported Au nanoparticle, using $\Delta\nu_{CO}$ for measurement. The Stark effect is related to electron donation to or withdrawal from frontier C−O orbitals and related to the k_{CO} force constant and the vibrational frequency, ν_{CO}.

A second effect related to electron donation or acceptance from a physisorbed donor or acceptor molecule has been studied on Au/TiO_2 catalysts and is schematically shown in Figure 2. Electron donors on TiO_2 will fill empty energy levels high in the bandgap region, which are due to the presence of empty lattice defect electron trap states. These levels are slightly below the bottom of the CB, such that the absorption of IR photons from an IR spectrometer is energetic enough to excite the trapped electrons to the CB. This excitation can be observed by means of the IR background rise for TiO_2 or Au/TiO_2 samples. Conversely, electron acceptors adsorbed on the surface will remove electrons from these bandgap states, causing a reduction of the IR background intensity. The effect is seen over much of the IR region because IR excitation occurs from electron trap states in the bandgap into electron continuum states in the CB.

In addition to CO/Au frequency shifts and the variation of the background IR intensity, the donation or acceptance of electrons to or from a semiconductor such as TiO_2 may be visualized through bending of the conduction and valence bands and the influence of such band bending on PL intensity. As shown schematically in Figure 3, a donor molecule will become positive and will result in the decrease of the extent of upward bending on an n-type TiO_2 surface, causing the PL emission region to expand forward nearer to the TiO_2 surface; an acceptor adsorbed on n-type TiO_2 will cause the bands to bend further upward, as additional negative charge is collected by the acceptor molecules causing the opposite effect on the thickness of the PL region and therefore decreasing the intensity of the PL signal. The change in band bending deduced by PL intensity is directly connected to the population change for trapped electrons in the bandgap states.

4.2. Electron Transfer from Adsorbate to TiO_2: Polarizability Correlation. The first step in the electron-transfer process involves the interaction between the adsorbates and the TiO_2 support. The electric field at the TiO_2 surface induces electronic polarization created by δ^+ polarization of hydrogen atoms in the donor molecules when near the surface of TiO_2. This magnitude of the adsorbate molecule polarization in the surface electric field on TiO_2 is proportional to α, the polarizability of the absorbate. In Table 1 the Stark shifts of $CO/Au/TiO_2$ influenced by donor molecules of variable polarizability, α, are compared. It is observed that the $\Delta\nu_{CO}$ shift responds in close proportion to the polarizability of the donor molecules employed on the TiO_2 surroundings to the Au particles.

Table 1. Relative Shifts of $\nu_{CO/Au}$ Compared to Absorbance Background Shifts in TiO_2 Due to Charge Transfer and to Polarizability (α)

donor molecule	$\Delta\nu_{CO}$ slope	α_{donor} ($Å^3$)[64]	$\Delta\nu_{CO}$ slope/$Å^3$	ΔIR bkg abs. slope	ΔIR slope/$Å^3$
CH_4	−1.11 (±0.1)	2.59	0.43 (±0.04)	0.00425	0.0016 (±0.0001)
C_2H_6	−2.09 (±0.1)	4.47	0.47 (±0.02)	0.00664	0.0015 (±0.0001)
C_3H_8	−2.79 (±0.1)	6.29	0.44 (±0.02)	0.00875	0.0014 (±0.0001)

DOI: 10.1021/ja511982n
J. Am. Chem. Soc. 2015, 137, 1972−1982

Another change noted in the IR spectra upon the adsorption of donor adsorbates onto the TiO_2 support is the increase in the IR background absorbance as shown in Figure 8. From previous studies,[58−60] this IR background absorbance increase (ΔIR) was attributed to electrons accumulating in discrete trap states just below the CB in TiO_2. Upon IR irradiation these electrons are excited into the CB continuum of states. We plotted the absorbance rise at 1900 cm^{-1} versus the donor coverage on TiO_2 and then calculated the linear slopes with respect to donor molecule coverage as shown in Figure 8a. The values are shown in Table 1 along with their corresponding ratios to donor molecule variable polarizability, α. Table 1 shows that both $\Delta\nu_{CO}/Å^3$ and $\Delta IR/Å^3$ are nearly the same for each different measurement, indicating that α is the driving force to the changes observed in both sets of spectroscopic measurements.

4.3. Electron Transfer from TiO_2 to Au: Behavior Uniformity of CO/Au IR Band. Once the electrons are transferred to or from the TiO_2, they move to or from the Au particles. In order to determine if the electron transfer is localized at the Au/TiO_2 interface or if the electrons are delocalized and transfer to the Au particle surface, the uniformity of the CO/Au IR frequency line shape as the adsorbates are added has to be determined. Each spectrum was analyzed using a best Lorenzian fit for the CO/Au IR absorbance band and the full width at half-maximum (FWHM) was recorded versus adsorbate coverage (see Figure S2). In addition, for all the donor and acceptor adsorption and desorption experiments, the observation of the band shift at 3 levels of cutting the band absorbance (1/4, 1/2, 3/4) shows clearly that a uniform shift of the overlapping ν_{CO} lines is observed and that a general shift of all lines is occurring. The FW accuracy is consistent with a uniform shift in the whole CO/Au IR line shape, meaning that slightly different CO bonding states respond uniformly to electron transfer from donor molecules to CO/Au.

Deshlahra et al.[65] analyzed the uniformity of the CO IR line shape for their system, which involved an applied dc voltage from a bias power supply to shift the ν_{CO} on Pt/TiO_2, in a different way. We followed their formula by subtracting the IR shifted spectra from the spectrum before donor adsorption (in our case) and then integrated the sum of the positive and negative peaks, $A_{difference}$. This value was then divided by the integrated area of the spectrum before donor adsorption, A_{total}. Therefore, the IR CO/metal frequency shift can be quantified by this ratio as shown in eq 1:

$$F = \frac{A_{difference}}{A_{total}} \quad (1)$$

where F is the fractional difference area.[65] We find F is linear versus donor coverage as seen in Figure S3 , and the F slopes for each donor scale proportionally with α_{donor}. From this analysis combined with FW measurements and DFT calculations shown in Figure 12c, we conclude that electron transfer into the Au produces a delocalized Gauss distribution of charge at the Au surface, to within the experimental errors of this investigation.

4.4. Stark Effect. The shift in the value of ν_{CO} can be envisioned as being due to the interaction of the chemisorbed CO molecule on a Au sphere with the transfer of donated electrons to the metal and then to the surface of the Au sphere, following the Gauss distribution of all added charge to the metal-sphere surface. The distribution of charge q over the low radius metal nanoparticle surface causes a high field at the sphere surface. The normal electric field strength E in vacuum near to the metal is given by eq 2:

$$E = \frac{q}{4\pi\varepsilon_0 r^2} \quad (2)$$

where q is the surface electron charge, ε_0 is the permittivity of free space, and r is the Au nanoparticle radius. Other measurements for CO adsorbed on a metal and exposed to various applied electric fields have yielded a Stark tuning rate of -8.6×10^{-9} $cm^{-1}/(V/m)$.[66] This Stark tuning model yields a value of $\Delta\nu_{CO}$ ~6 cm^{-1} per electron distributed on the 3 nm diameter Au particle surface. Our measurements of $\Delta\nu_{CO}$ = 1−3 cm^{-1}/monolayer of the three alkane donor molecules indicate that the range of Au charge transfer/monolayer of alkane is from 0.2−1 electron/Au particle. The DFT results reported in Figure 11 which showed charge transfer from adsorbed alkanes to TiO_2 and the subsequent transfer of charge to the Au atoms at the surface of nanoparticles are in general agreement with the Stark charge calculated from $\Delta\nu_{CO}$. In addition, we found that the explicit addition and removal of charge to the Au/TiO_2 system without donor or acceptor molecules, as is shown in Figure S4, also agrees closely with the Stark charge.

4.5. Support Effect: TiO_2 vs SiO_2. Our experiments have shown that semiconductor TiO_2 is effectively charged by either donor or acceptor molecules, whereas insulator SiO_2 is not. The dielectric constant, κ, is 80−100 for TiO_2[67,68] and only 3.9 for SiO_2.[68] TiO_2 therefore contains significant charge carriers related to defect sites in the bulk, whereas SiO_2 contains few charge carriers, making SiO_2 less affected by charge-transfer effects from donor or acceptor molecule adsorption, as shown in Figure 7. TiO_2 is therefore able to transfer charge to the surface of the Au nanoparticles, causing $\Delta\nu_{CO}$ effects, which are not observed for similar size Au nanoparticles on SiO_2. This observation verifies that CO molecules, adsorbed on Au nanoparticles, are sensitive "molecular voltmeters," which depend on the ability of the underlying semiconductor support to interact with polarizable molecules. Charge transfer to the support and hence to Au nanoparticles is observed by $\Delta\nu_{CO}$ shifts on Au nanoparticle detector sites.

5. CONCLUSIONS

1. IR and PL studies on ~3 nm Au particles on TiO_2 indicate that charge transfer from inert donor or acceptor molecules on semiconducting TiO_2 results in charging or discharging of the Au nanoparticles.
2. Charging of Au nanoparticles can be measured by careful studies of the frequency shift of adsorbed CO molecules. The sign and magnitude of the value of $\Delta\nu_{CO}$ are consistent with the Stark effect producing a surface electric field on Au nanoparticles. This is shown by DFT studies of Au nanoparticle charging and CO frequency effects and agrees well with the known Stark effect sensitivity of adsorbed CO. DFT studies further show that electric field effects from donor or acceptor molecules to adsorbed CO molecules do not occur through vacuum but via charge transfer into the oxide and onto the metal. The Au/TiO_2 catalysts are termed "molecular voltmeter" devices.
3. The value of $\Delta\nu_{CO}$ is proportional to the known polarizability, α, of three donor molecules, CH_4, C_2H_6,

DOI: 10.1021/ja511982n
J. Am. Chem. Soc. 2015, 137, 1972−1982

and C_3H_8, which adsorb only on the TiO_2 support by van der Waals interactions. The opposite effect takes place for the acceptor molecule, SF_6. Donor molecules on TiO_2 result in CO redshifts, and acceptor molecules result in CO blueshifts.

4. Charge transfer from physically adsorbed molecules to TiO_2 and then to Au nanoparticles occurs via electron storage in lattice defect states located in the TiO_2 bandgap near the bottom of the CB. The population of these defect electron trap states can be monitored by their broad IR excitation into the TiO_2 continuum. The magnitude of charge-transfer effects from TiO_2 into Au correlates with the occupancy of these defect electron trap states.
5. PL studies of C_3H_8 and SF_6 physisorbed molecules on pure TiO_2 confirm that these are electron-donor or -acceptor molecules which adsorb and desorb reversibly.
6. Charge transfer from donor or acceptor molecules on TiO_2, and from TiO_2 into Au depends upon significant carrier concentration changes associated with electron trap states in the TiO_2 semiconductor substrate. Insulator substrates (SiO_2) do not permit electron-transfer processes.

■ ASSOCIATED CONTENT

Supporting Information

Detailed difference analysis of CO IR shifts along with DFT calculations of electron transfer on Au/TiO_2 model catalysts and TEM images of the Au/TiO_2 catalyst. This material is available free of charge via the Internet at http://pubs.acs.org.

■ AUTHOR INFORMATION

Corresponding Author

*mlm4gf@virginia.edu

Notes

The authors declare no competing financial interest.

■ ACKNOWLEDGMENTS

We thank the DOE-Office of Basic Energy Sciences under grant no. DE-FGOZ-09ER16080 and the Army Research Office under grant no. W911NF-13-1-0101 for support of this research. We also thank AES Corporation for the AES Graduate Fellowships in Energy Research Program at the University of Virginia for Fellowships for Monica McEntee and Ana Stevanovic. We also gratefully thank the XSEDE computing resources from Texas Advanced Computing Center and San Diego Supercomputer Center for all of the DFT calculations. We last thank Matthew Reish for his insightful discussions and Matthew Schneider for his high-resolution TEM images of the Au/TiO_2 catalyst.

■ REFERENCES

(1) Smoluchowski, R. *Phys. Rev.* **1941**, *60*, 661.
(2) Gomer, R. *J. Chem. Phys.* **1953**, *21*, 1869−1876.
(3) Lang, N.; Kohn, W. *Phys. Rev. B* **1970**, *1*, 4555.
(4) Lang, N.; Kohn, W. *Phys. Rev. B* **1971**, *3*, 1215.
(5) Zhang, Z.; Yates, J. T., Jr. *Chem. Rev.* **2012**, *112*, 5520−5551.
(6) Mezhenny, S.; Maksymovych, P.; Thompson, T.; Diwald, O.; Stahl, D.; Walck, S.; Yates, J. T., Jr. *Chem. Phys. Lett.* **2003**, *369*, 152−158.
(7) Lüth, H. In Chapter 7: Space charge layers at semiconductor interfaces. *Surfaces and Interfaces of Solid Materials*, 3rd ed.; Springer: Berlin, 1997; pp 316−371.
(8) Ida, N. *Engineering electromagnetics*; Springer: Berlin, 2004; pp 173−281.
(9) Brundle, C. *Vibrations at Surfaces (Studies in Surface Science and Catalysis)*; Elsevier: Amsterdam, The Netherlands, 2000; pp 60−64.
(10) Wendt, S.; Sprunger, P. T.; Lira, E.; Madsen, G. K.; Li, Z.; Hansen, J. Ø; Matthiesen, J.; Blekinge-Rasmussen, A.; Lægsgaard, E.; Hammer, B. *Science* **2008**, *320*, 1755−1759.
(11) Stevanovic, A.; Büttner, M.; Zhang, Z.; Yates, J. T., Jr. *J. Am. Chem. Soc.* **2011**, *134*, 324−332.
(12) Anpo, M.; Tomonari, M.; Fox, M. A. *J. Phys. Chem.* **1989**, *93*, 7300−7302.
(13) Stevanovic, A.; Ma, S.; Yates, J. T., Jr. *J. Phys. Chem. C* **2014**, *118*, 21275−21280.
(14) Lambert, D. K. *Electrochim. Acta* **1996**, *41*, 623−630.
(15) Lambert, D. K. *J. Chem. Phys.* **1988**, *89*, 3847−3860.
(16) Korzeniewski, C.; Pons, S.; Schmidt, P.; Severson, M. *J. Chem. Phys.* **1986**, *85*, 4153−4160.
(17) Lambert, D. *Phys. Rev. Lett.* **1983**, *50*, 2106.
(18) Angell, C. L.; Schaffer, P. C. *J. Phys. Chem.* **1966**, *70*, 1413−1418.
(19) Banik, M.; El-Khoury, P. Z.; Nag, A.; Rodriguez-Perez, A.; Guarrottxena, N.; Bazan, G. C.; Apkarian, V. A. *ACS Nano* **2012**, *6*, 10343−10354.
(20) Li, L.; Steiner, U.; Mahajan, S. *Nano Lett.* **2014**, *14*, 495−498.
(21) Kamat, P. V.; Shanghavi, B. *J. Phys. Chem. B* **1997**, *101*, 7675−7679.
(22) Choi, H.; Chen, W. T.; Kamat, P. V. *ACS Nano* **2012**, *6*, 4418−4427.
(23) Ikeda, K.; Suzuki, S.; Uosaki, K. *J. Am. Chem. Soc.* **2013**, *135*, 17387−17392.
(24) McFarland, E. W.; Metiu, H. *Chem. Rev.* **2013**, *113*, 4391−4427.
(25) Metiu, H.; Chrétien, S.; Hu, Z.; Li, B.; Sun, X. *J. Phys. Chem. C* **2012**, *116*, 10439−10450.
(26) Zanella, R.; Giorgio, S.; Henry, C. R.; Louis, C. *J. Phys. Chem. B* **2002**, *106*, 7634−7642.
(27) Green, I. X.; Tang, W.; McEntee, M.; Neurock, M.; Yates, J. T., Jr. *J. Am. Chem. Soc.* **2012**, *134*, 12717−12723.
(28) Green, I. X.; Tang, W.; Neurock, M.; Yates, J. T., Jr. *Science* **2011**, *333*, 736−739.
(29) Jensen, H.; Joensen, K. D.; Jørgensen, J.; Pedersen, J. S.; Søgaard, G. *J. Nanopart. Res.* **2004**, *6*, 519−526.
(30) Li, G.; Gray, K. A. *Chem. Phys.* **2007**, *339*, 173−187.
(31) Zanella, R.; Sandoval, A.; Santiago, P.; Basiuk, V. A.; Saniger, J. M. *J. Phys. Chem. B* **2006**, *110*, 8559−8565.
(32) Basu, P.; Ballinger, T.; Yates, J. T., Jr. *Rev. Sci. Instrum.* **1988**, *59*, 1321−1327.
(33) Molina, L.; Rasmussen, M.; Hammer, B. *J. Chem. Phys.* **2004**, *120*, 7673.
(34) Laursen, S.; Linic, S. *Phys. Chem. Chem. Phys.* **2009**, *11*, 11006−11012.
(35) Green, I. X.; Tang, W.; Neurock, M.; Yates, J. T., Jr. *Angew. Chem., Int. Ed.* **2011**, *50*, 10186−10189.
(36) Kresse, G. *Phys. Rev. B* **2000**, *62*, 8295.
(37) Kresse, G.; Joubert, D. *Phys. Rev. B* **1999**, *59*, 1758.
(38) Blöchl, P. E. *Phys. Rev. B* **1994**, *50*, 17953.
(39) Perdew, J. P.; Wang, Y. *Phys. Rev. B* **1992**, *45*, 13244.
(40) Dudarev, S.; Botton, G.; Savrasov, S.; Humphreys, C.; Sutton, A. *Phys. Rev. B* **1998**, *57*, 1505.
(41) Morgan, B. J.; Watson, G. W. *Surf. Sci.* **2007**, *601*, 5034−5041.
(42) Monkhorst, H. J.; Pack, J. D. *Phys. Rev. B* **1976**, *13*, 5188.
(43) Kerber, T.; Sierka, M.; Sauer, J. *J. Comput. Chem.* **2008**, *29*, 2088−2097.
(44) Bader, R. F. *Atoms in Molecules: A Quantum Theory*; Oxford University Press: New York, 1990.
(45) Tang, W.; Sanville, E.; Henkelman, G. *J. Phys.: Condens. Matter* **2009**, *21*, 084204.
(46) Dekkers, M.; Lippits, M.; Nieuwenhuys, B. *Catal. Lett.* **1998**, *56*, 195−197.
(47) Chen, M.; Goodman, D. *Science* **2004**, *306*, 252−255.

DOI: 10.1021/ja511982n
J. Am. Chem. Soc. 2015, 137, 1972−1982

(48) Hao, Y.; Mihaylov, M.; Ivanova, E.; Hadjiivanov, K.; Knözinger, H.; Gates, B. *J. Catal.* **2009**, *261*, 137−149.
(49) Schreiber, H.; McIntosh, R. *Can. J. Chem.* **1955**, *33*, 259−267.
(50) Bandara, A.; Abu-Haija, M.; Höbel, F.; Kuhlenbeck, H.; Rupprechter, G.; Freund, H. *Top. Catal.* **2007**, *46*, 223−230.
(51) Fichthorn, K. A.; Miron, R. A. *Phys. Rev. Lett.* **2002**, *89*, 196103.
(52) Tait, S. L.; Dohnalek, Z.; Campbell, C. T.; Kay, B. D. *J. Chem. Phys.* **2006**, *125*, 234308.
(53) Hägglund, C.; Kasemo, B.; Österlund, L. *J. Phys. Chem. B* **2005**, *109*, 10886−10895.
(54) Goyal, S.; Schutt, D.; Scoles, G. *Phys. Rev. Lett.* **1992**, *69*, 933.
(55) Rosenbaum, A.; Freedman, M.; Sibener, S. *J. Phys. Chem. A* **2006**, *110*, 5537−5541.
(56) Ogawa, T.; Mochiji, K.; Ochiai, I.; Yamamoto, S.; Tanaka, K. *J. Appl. Phys.* **1994**, *75*, 4680−4685.
(57) Yoshihara, T.; Katoh, R.; Furube, A.; Tamaki, Y.; Murai, M.; Hara, K.; Murata, S.; Arakawa, H.; Tachiya, M. *J. Phys. Chem. B* **2004**, *108*, 3817−3823.
(58) Panayotov, D. A.; Burrows, S. P.; Yates, J. T., Jr.; Morris, J. R. *J. Phys. Chem. C* **2011**, *115*, 22400−22408.
(59) Panayotov, D. A.; Yates, J. T., Jr. *Chem. Phys. Lett.* **2007**, *436*, 204−208.
(60) Panayotov, D. A.; Yates, J. T., Jr. *J. Phys. Chem. C* **2007**, *111*, 2959−2964.
(61) Willis, R. L.; Olson, C.; O'Regan, B.; Lutz, T.; Nelson, J.; Durrant, J. R. *J. Phys. Chem. B* **2002**, *106*, 7605−7613.
(62) Sezen, H.; Buchholz, M.; Nefedov, A.; Natzeck, C.; Heissler, S.; Di Valentin, C.; Wöll, C. *Sci. Rep.* **2014**, *4*, 3808.
(63) Anpo, M.; Chiba, K.; Tomonari, M.; Coluccia, S.; Che, M.; Fox, M. A. *Bull. Chem. Soc. Jpn.* **1991**, *64*, 543−551.
(64) Boyd, R.; Kesner, L. *Macromolecules* **1987**, *20*, 1802−1806.
(65) Deshlahra, P.; Schneider, W. F.; Bernstein, G. H.; Wolf, E. E. *J. Am. Chem. Soc.* **2011**, *133*, 16459−16467.
(66) Lambert, D. *Stud. Surf. Sci. Catal.* **1983**, *14*, 59−64.
(67) Kim, S. K.; Kim, W.; Kim, K.; Hwang, C. S.; Jeong, J. *Appl. Phys. Lett.* **2004**, *85*, 4112−4114.
(68) Robertson, J. *Rep. Prog. Phys.* **2006**, *69*, 327.

DOI: 10.1021/ja511982n
J. Am. Chem. Soc. 2015, 137, 1972−1982